SF2A 2023
M. N'Diaye, A. Siebert, N. Lagarde, O. Venot, K. Baillié, M. Béthermin, E. Lagadec, J. Malzac, J. Richard (eds)

A NEW SCENARIO FOR MAGNETAR FORMATION IN A PROTO-NEUTRON STAR SPUN UP BY FALLBACK

P. Barrere[1], J. Guilet[1], R. Raynaud[2] and A. Reboul-Salze[3]

Abstract. The origin of magnetar magnetic field is a challenging question. In situ magnetic field amplification by dynamo action is a promising process to generate ultra-strong magnetic fields in fast-rotating progenitors. It is, however, unclear whether the fraction of progenitors harboring fast core rotation is sufficient to explain the entire magnetar population. To address this point, we investigate a new scenario for magnetar formation from a slow rotating progenitor, in which a slow-rotating proto-neutron star is spun-up by the supernova fallback. We show that this can trigger the development of the Tayler-Spruit dynamo while other dynamo processes are disfavored. In this proceeding, we present an analytical model of our scenario and three dimensional numerical simulations of the Tayler-Spruit dynamo. We find that the generated magnetic field intensities are close to those expected in magnetars and our simulations demonstrate the existence of the Tayler-Spruit dynamo in the frame of this scenario. Thus, our scenario provides a new promising approach to form magnetars from slow-rotating progenitors.

Keywords: magnetars, supernovae, magnetohydrodynamics (MHD), instabilities, methods: numericals

1 Introduction

Magnetars are isolated young neutron stars characterized by the most intense magnetic fields known in the Universe, which power a wide diversity of outstanding emissions. Under the assumption of a magnetic dipole braking, the observations of the rotation period and its derivative, i.e. the spin-down, show that magnetars harbor a typical surface magnetic dipole of $\sim 10^{14} - 10^{15}$ G (Rea et al. 2012; Olausen & Kaspi 2014). Magnetars with a millisecond rotation period may also be at the origin of extreme explosions, which are more energetic than typical supernovae : (i) hypernovae (e.g. Duncan & Thompson 1992; Gompertz & Fruchter 2017; Metzger et al. 2011, 2018) via a magnetorotational explosion (e.g. Dessart et al. 2008; Obergaulinger & Aloy 2022; Bugli et al. 2021, 2023), and (ii) superluminous supernovae through a delayed energy injection from the spin-down luminosity (e.g. Woosley 2010; Inserra et al. 2013; Nicholl et al. 2013).

The formation of magnetar magnetic field is therefore a critical question to understand magnetar activity and extreme explosions. Two scenarios invoke the amplification of the magnetic field via a dynamo action during the early stages of the proto-neutron star (PNS): the convective dynamo scenario (e.g. Thompson & Duncan 1993; Raynaud et al. 2020, 2022) and the magnetorotational instability (MRI) scenario (e.g. Reboul-Salze et al. 2021, 2022; Guilet et al. 2022). They both suppose a PNS with a millisecond rotation period which stems from the rotation of the progenitor core. However, it is still uncertain whether there is a large enough fraction of fast rotating progenitor cores to explain the formation of whole magnetar population, which represents $\sim 10 - 40\,\%$ of the young neutron star population (e.g. Kouveliotou et al. 1994; Beniamini et al. 2019).

This proceeding presents a new magnetar formation scenario in which the PNS rotation is determined by the fallback accretion and the magnetic field amplified via the Tayler-Spruit dynamo (Barrère et al. 2022, 2023). This dynamo is driven by the instability of a toroidal magnetic field, called the Tayler instability (Tayler 1973; Goossens & Tayler 1980; Goossens 1980; Goossens et al. 1981) and was first modelled by Spruit (2002). An alternative modelling is proposed Fuller et al. (2019) to tackle critics of Spruit's model (see Denissenkov & Pinsonneault 2007; Zahn et al. 2007). This mechanism is usually invoked in the context of angular momentum transport in stellar radiative zones (e.g. Eggenberger et al. 2005, 2019; Cantiello et al. 2014; Griffiths et al. 2022) and we apply it in the context of magnetar formation for the first time (Barrère et al. 2022, 2023).

[1] Université Paris-Saclay, Université Paris Cité, CEA, CNRS, AIM, 91191, Gif-sur-Yvette, France
[2] Université Paris Cité, Université Paris-Saclay, CEA, CNRS, AIM, 91191, Gif-sur-Yvette, France
[3] Max Planck Institute for Gravitational Physics (Albert Einstein Institute), 14476 Potsdam, Germany

2 New magnetar formation model (Barrère et al. 2022)

As illustrated in Figure 1, our magnetar formation scenario begins $\sim 10\,$s after the collapse of the progenitor core when a fraction of the initially ejected matter which is still gravitationally bound to the PNS is accreted onto the PNS surface. This fallback accretion is found to be asymmetric (Chan et al. 2020) and the matter is expected to have an angular momentum comparable to the Keplerian angular momentum (Janka et al. 2022). The PNS surface is therefore spun up, which creates a differential rotation with the PNS surface rotating faster than the core. We argue that the other dynamo mechanisms are disfavored* and that only the Tayler-Spruit dynamo development is triggered: (i) the differential rotation shears the axisymmetric poloidal magnetic field B_r into an axisymmetric toroidal magnetic field B_ϕ (ii) until the latter becomes Tayler unstable, which creates a perturbed non-axisymmetric field $\delta B_\perp$ and (iii) generates B_r via a non-linear induction characterized by the azimuthal component of the electromotive force E_ϕ. The dynamo loop amplifies the magnetic field until a turbulent dissipation due to the instability balances the growth of the magnetic field, which makes the dynamo saturate. Two descriptions of the saturation mechanisms have been proposed: that of (Spruit 2002) and (Fuller et al. 2019), which are both still keenly discussed in particular due to the difficulty in finding the dynamo in direct numerical simulations (Denissenkov & Pinsonneault 2007; Zahn et al. 2007; Petitdemange et al. 2023; Barrère et al. 2023).

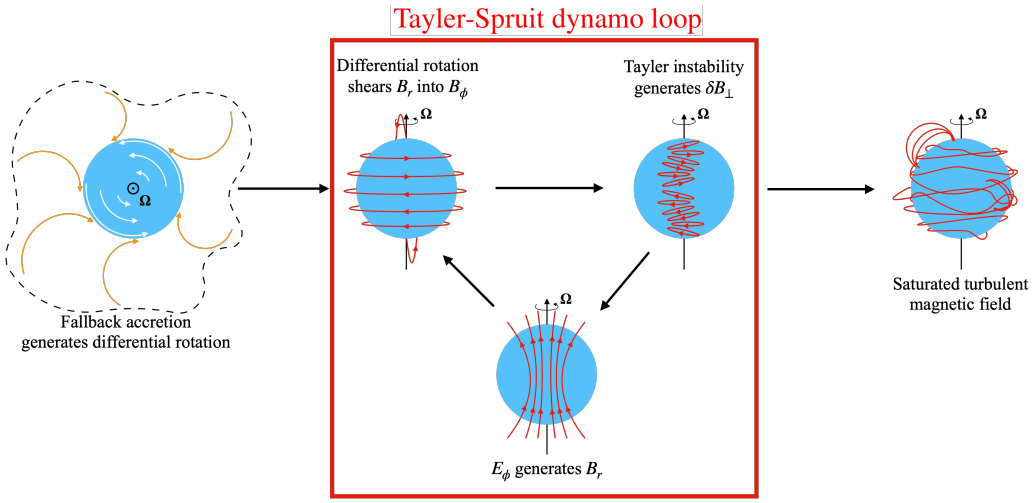

Fig. 1. Schematic representation of the different stages of our magnetar formation scenario. The dashed line encloses the region of the fallback (orange arrows). Red and white lines represent the magnetic field lines and fluid motions, respectively. Ω and E_ϕ stand for the angular rotation frequency and the azimuthal component of the electromotive force, respectively. B_ϕ and B_r are the axisymmetric azimuthal and radial magnetic fields, and $\delta B_\perp$ is the non-axisymmetric perpendicular magnetic field.

To check the plausibility of this scenario to form magnetars, we built a one-zone model. It consists in a system of average time evolution equations for the rotational properties of the PNS: average rotation rate Ω and shear rate q, and different components of the magnetic field: B_ϕ, B_r, $\delta B_\perp$ using the formalism of Fuller et al. (2019) to describe the Tayler-Spruit dynamo. The integration of these equations for specific values of the total accreted mass (which is equivalent to choose a value for the PNS final rotation rate) show a time evolution of the magnetic field which is consistent with the phases of our scenario from the shearing to the saturation (see Fig. 2 and 3 in Barrère et al. 2022). To define a proxy for the saturated magnetar magnetic field, we used the maximum magnetic intensity reached (plus signs in figure 2) and the magnetic intensity when $q = 0$, i.e. when all the rotation becomes rigid due to angular momemtum transport (cross signs in figure 2). We see that the measured saturated B_ϕ (in blue) and B_r (in green) are close to the analytical predictions of Fuller et al. (2019) (in solid line) and that the saturated B_r crosses the regions of magnetic fields expected for magnetars (in darkgrey) for rotation periods $\lesssim 28\,$ms (or a total accreted mass $\gtrsim 10^{-2}\,\mathrm{M}_\odot$), which is then the lower rotation

*Indeed, the PNS interior is expected to be mostly stably stratified when the fallback occurs (Hüdepohl 2014) and the MRI only develops when the rotation rate decreases with the radius.

period limit to form magnetars with our scenario. In the same figure, a comparison is also made with the predictions of Spruit (2002), from which we can also infer a lower limit for rotation period of ~ 8 ms. Our model therefore predicts that strong enough magnetic fields can be generated to form magnetars in our scenario.

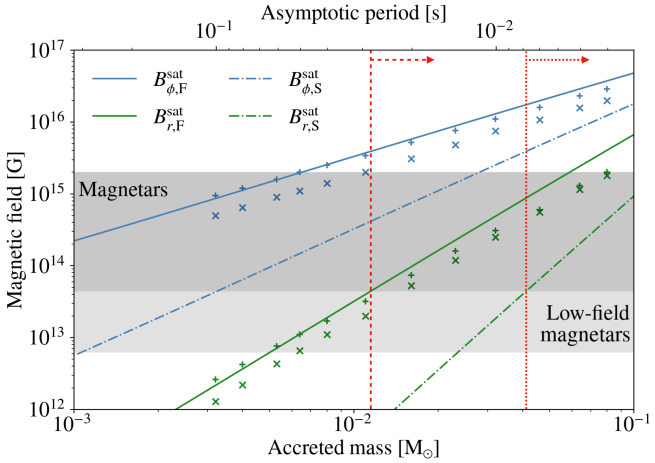

Fig. 2. Different characteristic timescales as a function of the accreted mass: winding (black), Tayler instability (dark blue), and dynamo (red). The green line represents the sum of the three timescales. The shear rate is set at $q = 1$. The green crosses represent the entire amplification time obtained by integrating the evolution equations. The red vertical line shows the lower limit of the accreted mass to form a magnetar with a radial field stronger than $B_Q \equiv m_e c^2/e\hbar \simeq 4.4 \times 10^{13}$ G using the predictions of Fuller et al. (2019).

3 3D numerical simulations (Barrère et al. 2023)

The promising results of the semi-analytical model of Barrère et al. (2022) encourages further studies of our scenario, especially through numerical simulations. Indeed, a numerical study would test whether the Tayler instability can sustain a dynamo, in particular in the framework of our scenario. In the case where the Tayler-Spruit dynamo is present, numerical simulations would also provide information about the geometry the magnetic field and the scaling law it follows.

We performed three-dimensional (3D) direct numerical simulations of a stably stratified and electrically conducting Boussinesq fluid with the pseudo-spectral code MagIC (Wicht 2002; Gastine & Wicht 2012). The fluid has a constant density $\rho = 3.8 \times 10^{14}\,\mathrm{g\,cm^{-3}}$ (which corresponds to a proto-neutron star mass of $M = 1.4\,\mathrm{M_\odot}$) and evolves between two concentric spheres of radius $r_i = 3$ km and $r_o = 12$ km, rotating at the angular frequencies Ω_i and $\Omega_o = 200\,\mathrm{rad\,s^{-1}}$, respectively. The imposed differential rotation is characterized by the Rossby number $Ro \equiv 1 - \Omega_i/\Omega_o > 0$, which is varied between 0.125 and 1.2. In all the simulations, we keep fixed the other dimensionless control parameters: the shell aspect ratio $\chi \equiv r_i/r_o = 0.25$, the thermal and magnetic Prandtl numbers $Pr \equiv \nu/\kappa = 0.1$ and $Pm \equiv \nu/\eta = 1$, respectively, the Ekman number $E \equiv \nu/(d^2\Omega_o) = 10^{-5}$, and the ratio of the Brunt-Väisälä to the outer angular frequency $N/\Omega_o = 0.1$. The coefficients ν, κ, η, and $d \equiv r_o - r_i$ are respectively the kinematic viscosity, the thermal diffusivity, the resistivity, and the shell width. The magnetic energy is measured by the Elsasser number $\Lambda \equiv B^2_{\rm rms}/(4\pi\rho\eta\Omega_o)$.

The performed simulation are all gathered in a diagram which displays the average magnetic energy during the saturated state of the dynamo (measured by the Elsasser number) as a function of the input differential rotation (represented by the Rossby number). This diagram, called *bifurcation diagram*, (plot on the left in figure 3) shows different branches represented by different colours. Following the bifurcation diagram, when Ro is low, the flow can not amplify an initially weak magnetic field ($\Lambda = 1 \times 10^{-4}$) until $Ro \sim Ro_{\rm W} = 0.65$ is reached, where an exponential amplification occurs until saturation at $\Lambda \sim 3 \times 10^{-1}$. This dynamo branch (in black) is driven by an hydrodynamic instability, which occurs for $Ro \gtrsim Ro_{\rm hyd} = 0.177$. For $Ro \gtrsim 0.8$, the magnetic field undergoes a non-linear growth and transitions to another dynamo branch (in green) at $\Lambda \sim 10$. Restarting from nearby saturated states, the branch can be extended to $Ro \sim 0.37 < Ro_{\rm W}$, which betrays the subcriticality of the branch. Finally, a stronger branch at $\Lambda \sim 80$ (in red) can be reached by starting with a strong magnetic field of $\Lambda \sim 10$ and be maintained to $Ro \sim Ro_{\rm D} = 0.19$. These three main solutions not only

differs by their magnetic strength but also by their geometry (see snapshots on the right of 3): equatorial, hemispherical, and dipolar (i.e. equatorially symmetric magnetic field), respectively.

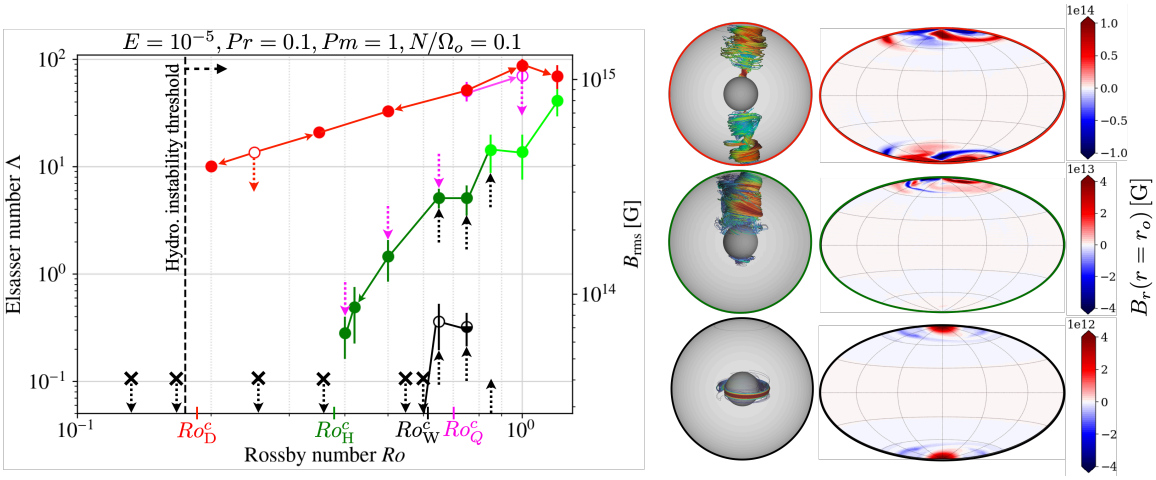

Fig. 3. Left: Bifurcation diagram of the time and volume averaged Elsasser number (and rms magnetic field) versus the Rossby number. Distinct dynamo branches are represented: dipolar (red), quadrupolar (mauve), hemispherical (green), and kinematic (black) whose respective thresholds are $Ro^c_{\rm D} \sim 0.19$, $Ro^c_{\rm Q} \sim 0.7$, $Ro^c_{\rm H} \sim 0.37$, and $Ro^c_{\rm W} \sim 0.62$. The hydrodynamic instability is triggered for $Ro^c_{\rm hyd} > 0.177$. Dark green circles are stationary hemispherical dynamos and light green ones display parity modulations. Black crosses indicate failed dynamos, empty circles metastable solutions. Arrows attached to circles indicate the initial condition of the associated simulation. The black half empty circle specifies that the solution was found to be metastable in a simulation and stable in another. The error bars indicate the standard deviation. **Right:** snapshots of the magnetic field lines and surface radial fields associated to the different main dynamo branches at $Ro = 0.75$: dipolar (top), hemispherical (middle), and kinematic (bottom).

Furthermore, we show that both hemispherical and dipolar dynamos are driven by the Tayler instability: (i) the magnetic field is clearly dominated by its axisymmetric toroidal component, (ii) snapshots of the perturbed magnetic field and magnetic energy spectra show a kink-shape instability (i.e. $m = 1$ perturbation), and (iii) the transition from the kinematic to the hemispherical branch occurs when the axisymmetric toroidal field exceeds the critical strength of the Tayler instability (see Barrère et al. 2023). Finally, the measure of the shear rate in our simulations shows that the hemispherical and dipolar branches follow the respective theoretical predictions of Spruit (2002) and Fuller et al. (2019).

4 Conclusions

To conclude, we propose a new magnetar formation scenario, in which the magnetic field amplified by the Tayler-Spruit dynamo in a slowly rotating and weakly magnetized PNS spun up by fallback. The semi-analytical modelling of our scenario built in Barrère et al. (2022) predicts that our scenario can form magnetars for PNS spun up to $\lesssim$ 28 ms rotation periods, which is greater than the expected rotation period for proto-magnetars born in typical supernovae (e.g. Vink & Kuiper 2006). Our numerical study in Barrère et al. (2023) demonstrates the existence of two distinct Tayler-Spruit dynamos which differ by their magnetic field strength, equatorial symmetry (hemispherical and dipolar), and scaling law. Besides, the study shows that both theoretical predictions of Spruit (2002) and Fuller et al. (2019) can be found in direct numerical simulations. This study is therefore complementary with Petitdemange et al. (2023), which finds a dynamo similar to the Tayler-Spruit dynamo of Spruit (2002) but in the context of stellar radiative zones and so with an opposite differential rotation. Finally, by extrapolating our results for the dipolar branch to $q \sim 1$ as in Barrère et al. (2022), we obtain a magnetic dipole of $B_{\rm dip} \sim 3.2 \times 10^{14}$ G, which falls right in the magnetar range (Olausen & Kaspi 2014). Extended parameter studies of the impact of the stratification and the resistivity on the dynamo will be needed to better constrain the astrophysical implications and test the theoretical predictions. Overall, by deepening our understanding on the complex dynamics of the Tayler-Spruit dynamo, our results are of particular importance in the domains of dynamo theory, stellar evolution modelling and magnetar formation.

This research was supported by the European Research Council through the ERC starting grant MagBURST No. 715368 and the PNPS and the PNHE programs of CNRS/INSU, co-funded by CEA and CNES. Numerical simulations have been carried out at the CINES on the Jean-Zay supercomputer (DARI project A0130410317). We are grateful to H.-T. Janka for his contribution to the article Barrère et al. (2022) and T. Foglizzo, A. Igoshev, L. Petitdemange, C. Gissinger, and F. Daniel for useful discussions.

References

Barrère, P., Guilet, J., Raynaud, R., & Reboul-Salze, A. 2023, arXiv e-prints, arXiv:2306.12296
Barrère, P., Guilet, J., Reboul-Salze, A., Raynaud, R., & Janka, H. T. 2022, Astron. Astrophys., 668, A79
Beniamini, P., Hotokezaka, K., van der Horst, A., & Kouveliotou, C. 2019, Mon. Not. Astron. R. Soc., 487, 1426
Bugli, M., Guilet, J., Foglizzo, T., & Obergaulinger, M. 2023, Mon. Not. Astron. R. Soc., 520, 5622
Bugli, M., Guilet, J., & Obergaulinger, M. 2021, Mon. Not. Astron. R. Soc., 507, 443
Cantiello, M., Mankovich, C., Bildsten, L., Christensen-Dalsgaard, J., & Paxton, B. 2014, Astrophys. J., 788, 93
Chan, C., Müller, B., & Heger, A. 2020, Mon. Not. Astron. R. Soc., 495, 3751
Denissenkov, P. A. & Pinsonneault, M. 2007, Astrophys. J., 655, 1157
Dessart, L., Burrows, A., Livne, E., & Ott, C. D. 2008, Astrophys. J. Lett., 673, L43
Duncan, R. C. & Thompson, C. 1992, Astrophys. J. Lett., 392, L9
Eggenberger, P., den Hartogh, J. W., Buldgen, G., et al. 2019, Astron. Astrophys., 631, L6
Eggenberger, P., Maeder, A., & Meynet, G. 2005, Astron. Astrophys., 440, L9
Fuller, J., Piro, A. L., & Jermyn, A. S. 2019, Mon. Not. Astron. R. Soc., 485, 3661
Gastine, T. & Wicht, J. 2012, Icarus, 219, 428
Gompertz, B. & Fruchter, A. 2017, Astrophys. J., 839, 49
Goossens, M. 1980, Geophysical and Astrophysical Fluid Dynamics, 15, 123
Goossens, M., Biront, D., & Tayler, R. J. 1981, Astrophys. Space Sci., 75, 521
Goossens, M. & Tayler, R. J. 1980, MNRAS, 193, 833
Griffiths, A., Eggenberger, P., Meynet, G., Moyano, F., & Aloy, M.-Á. 2022, Astron. Astrophys., 665, A147
Guilet, J., Reboul-Salze, A., Raynaud, R., Bugli, M., & Gallet, B. 2022, Mon. Not. Astron. R. Soc., 516, 4346
Hüdepohl, L. 2014, PhD thesis, Technical University of Munich, Germany
Inserra, C., Smartt, S. J., Jerkstrand, A., et al. 2013, Astrophys. J., 770, 128
Janka, H.-T., Wongwathanarat, A., & Kramer, M. 2022, Astrophys. J., 926, 9
Kouveliotou, C., Fishman, G. J., Meegan, C. A., et al. 1994, Nature, 368, 125
Metzger, B. D., Beniamini, P., & Giannios, D. 2018, Astrophys. J., 857, 95
Metzger, B. D., Giannios, D., Thompson, T. A., Bucciantini, N., & Quataert, E. 2011, Mon. Not. Astron. R. Soc., 413, 2031
Nicholl, M., Smartt, S. J., Jerkstrand, A., et al. 2013, Nature, 502, 346
Obergaulinger, M. & Aloy, M. Á. 2022, Mon. Not. Astron. R. Soc., 512, 2489
Olausen, S. A. & Kaspi, V. M. 2014, Astrophys. J.s, 212, 6
Petitdemange, L., Marcotte, F., & Gissinger, C. 2023, Science, 379, 300
Raynaud, R., Cerdá-Durán, P., & Guilet, J. 2022, Mon. Not. Astron. R. Soc., 509, 3410
Raynaud, R., Guilet, J., Janka, H.-T., & Gastine, T. 2020, Sci. Adv., 6, eaay2732
Rea, N., Israel, G. L., Esposito, P., et al. 2012, Astrophys. J., 754, 27
Reboul-Salze, A., Guilet, J., Raynaud, R., & Bugli, M. 2021, Astron. Astrophys., 645, A109
Reboul-Salze, A., Guilet, J., Raynaud, R., & Bugli, M. 2022, Astron. Astrophys., 667, A94
Spruit, H. C. 2002, Astron. Astrophys., 381, 923
Tayler, R. J. 1973, Mon. Not. Astron. R. Soc., 161, 365
Thompson, C. & Duncan, R. C. 1993, Astrophys. J., 408, 194
Vink, J. & Kuiper, L. 2006, Mon. Not. Astron. R. Soc., 370, L14
Wicht, J. 2002, Physics of the Earth and Planetary Interiors, 132, 281
Woosley, S. E. 2010, Astrophys. J. Lett., 719, L204
Zahn, J. P., Brun, A. S., & Mathis, S. 2007, Astron. Astrophys., 474, 145